Ionic Thermoelectric Effect Inducing Cation Enriched Surface of Hydrogel to Enhance Output Performance of Triboelectric Nanogenerator

Yizhong Chen[a], Chaosheng Shi[a], Jingfei Zhang[a], Yongqiang Dai[a], Yu Su[a], Bing Liao[b], Mingqiu Zhang[c], Xiaoming Tao[d], Wei Zeng[a*]

a Guangdong Key Laboratory of Industrial Surfactant, Institute of Chemical Engineering, Guangdong Academy of Sciences, Guangzhou 510665, P. R. China
b Guangdong Academy of Sciences, Guangzhou 510070, P. R. China
c Key Laboratory for Polymeric Composite and Functional Materials of Ministry of Education, GD HPPC Lab, School of Chemistry and Chemical Engineering, Sun Yat-Sen University, Guangzhou 510275, P. R. China
d Research Centre for Smart Wearable Systems, Institute of Textiles and Clothing, The Hong Kong Polytechnic University, Hong Kong
*Corresponding author. E-mail address: zengwei@gdcri.com (W. Zeng)

ABSTRACT

The most robust consensus related to ionic hydrogel based triboelectric nanogenerator (TENG) is that the charge density at the solid interface plays a pivotal role on its output performance. However, there has been no reliable evidence of the mechanism regarding the influence for ion enrichment on TENG. Higher surface charge density at the solid interface could result in higher output performance when well controlling the charge density at the ionic hydrogel surface. Herein, the ionic hydrogel was prepared through polymerization reaction of the organic monomers with LiCl as the ionic conductor. The ion migration on the hydrogel surface was regulated via tuning the temperature difference between the top and bottom sides. Upon contacting with the upper electrode, more induction charges were induced on the cation enriched surface of hydrogel, leading to a larger output of the TENG. At the temperature difference of 25 °C, the open circuit voltage and maximum output power density increased by 77 % and 166 % compared with the TENG without temperature field, respectively. When the temperature of hydrogel surface was higher than 50 °C, the output performance of TENG would decrease due to the water loss of hydrogel. This research will advance further understanding of the mechanism of thermoelectric

ionic conductors in TENGs, self-powered sensors and wearable devices.

Keywords: Triboelectric nanogenerator; thermoelectric materials; hydrogel;

1. Introduction

With the rapid development of information era, a series of intelligent electronics including wearable devices, consumer electronics, intelligent robots and the internet of things have more and more promoting effect on people's daily lives [1-6]. However, continuous power supply remains a challenge for devices and supporting circuits in practical scenarios, which is also the key problem in the field of internet of things [7-9]. At present, battery is regarded as the most commonly used power supplier, due to its simple preparation and low-cost, yet it suffers from several major drawbacks: limited lifespan, difficulty in power monitoring and requirement for regular replacement [10, 11]. Fortunately, self-powered devices might be a better substitute for batteries. They can work continuously without external power supply derived from their ability to harvest kinds of energy from the surrounding environment and convert it into electrical energy to power their own sensing units [12, 13]. Besides, self-powered devices are environmentally friendly and portable with low cost and long service life. Integrating self-powered devices into the system, the design complexity can be greatly reduced, and the distribution range and integration can continue to be improved.

Triboelectric nanogenerator (TENG) has become as a worldwide research hotspot due to its light weight, low cost and wide range of materials [14-20]. Relying on the coupling effect of friction electrification and electrostatic induction, TENG can transform the environmental mechanical energy into electrical energy. Therefore, it has great application potential in energy harvesting and self-powered sensing [14, 21, 22]. Friction driven by external force results in two surfaces involved carrying opposite static charges. Upon separation, the potential difference between the surfaces will drive the flow of electrons in the external circuit, resulting in a current output. TENG has been explored and applied in many fields, including sensing, implantable power supply, healthcare and biomedical applications. The output performance of TENG is heavily dependent on the surface charge density of the friction material [23-25]. Hence, it becomes important to control the interface charge density by changing the properties of friction materials. [16, 26, 27].

Hydrogels with three-dimensional network structures have excellent mechanical properties, including high ductility, flexibility, elasticity and biocompatibility [28, 29] which equip them with great potential to be applied in TENG [30, 31]. In recent years, researchers have explored the application of hydrogels in TENG. Xu et al. [32] reported a flexible TENG collecting mechanical energy from a variety of human movements. The energy collected in turn can be used in self-powered human motion sensors, opening up new research directions for ionic hydrogel-based TENG. On the other hand, Pu et al. [33] reported friction-generated self-powered pressure sensors by using ionic hydrogels as electrodes, which shows a sensitivity of 0.013 kPa^{-1} and a minimum pressure measurement limit to 1.3 kPa. It is worth noting that, the friction dielectric material in TENG is still the elastomer encapsulating hydrogel, rather than the hydrogel itself. Currently, ionic hydrogels normally act as flexible conductive electrodes that are connected with metal conductors, and drive electrons in external circuits to generate electrical signals. So far, however, when ionic hydrogel is directly used as a friction dielectric material, only a few studies refer to the mechanism of the movement of cations and anions in the hydrogel and the effect of the hydrogel surfaces with enriched cations and anions on triboelectrification. Generally, the diffusion of cations and anions in ionic hydrogels can be driven by the Soret effect under a temperature difference [34-36], and the cations and anions accumulate at the low and high temperature ends respectively, which gives rise to the ion concentration gradient and the corresponding thermal voltage [37]. Our previous study has indicated that an ionic hydrogel fabricated with Li_2SO_4 as a conductive ionic compound has a thermoelectric coefficient up to 11.5 $mV \cdot K^{-1}$ [38]. Therefore, the enrichment of cations and anions on the hydrogel surface can be obtained by the potential difference between its two ends in the temperature field. Further considering the diffusion of cations and anions in ionic hydrogels under temperature difference, this also can enhance the surface charge density and result an improved output performance of ionic hydrogel based TENG.

Herein, ionic hydrogels with thermoelectric properties were prepared as the friction dielectric material by adjusting the three-dimensional network structure of the hydrogel and the type of cations and anions. The TENG was then designed with the hydrogels on ion-enriched surfaces as the friction material. This TENG presented an open voltage of 22 V when applied a force of 90 N without temperature difference.

Interestingly, benefited from the higher ionic density at the interface of TENG, the open circuit voltage and maximum output power density increased by 77 % and 166 % at the temperature difference of 25 °C. Furthermore, the corresponding electrification mechanism was studied and the application of TENG was discussed. All the results proved the great application prospect of the as-prepared TENG in the self-powered wearable electronics and sensors.

2. Results and Discussion

2.1. Chemical Structure of Ionic Hydrogel

The preparation process of the ionic hydrogel was schematically illustrated in Figure 1 (a). The hydrogel structure consists of the chemical cross-linking network formed by polymerization reaction of acrylamide (AM) monomer and the second complex network formed by the complexation of carboxyl groups on sodium alginate (SA) molecule with calcium ions. The lithium chloride was dissolved in water acting as ion source.

The chemical structures of fabricated hydrogel compound and AM monomer were characterized by Fourier transform infrared spectra (FTIR) as shown in Figure 1 (b). The bands at 3352 and 3185 cm^{-1} are ascribed to the stretching vibration of NH_2, while bands located at 1674 and 1612 cm^{-1} are attributed to the stretching vibration of amide. The band observed at 1428 cm^{-1} belongs to the bending vibration of CH_2. Most importantly, the bands at 3033, 988 and 964 cm^{-1} ascribed to the double bonds of AM disappeared during the formation of hydrogel, indicating the successful polymerization of AM monomers [39, 40].

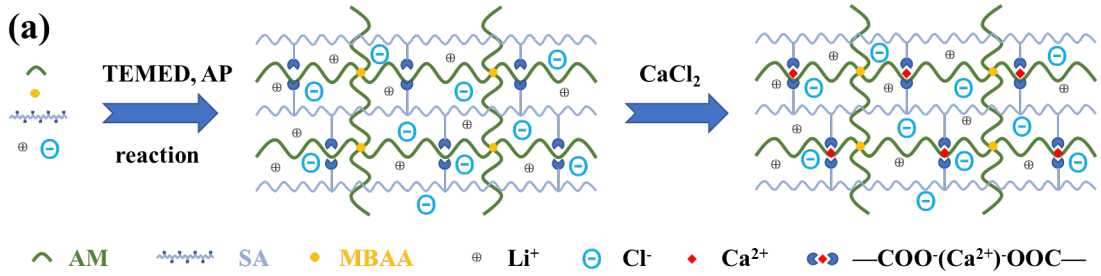

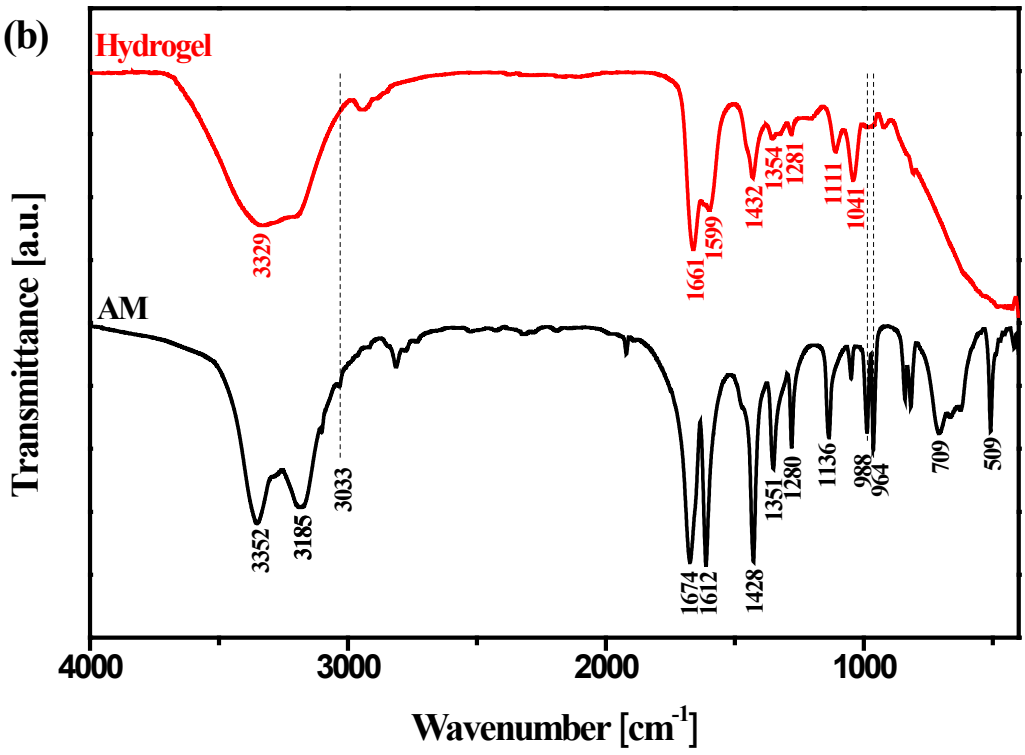

Figure 1. (a) Schematic diagram of the preparation process of the ionic hydrogel. (b) FTIR spectrum of AM and ionic hydrogel.

2.2. Thermoelectric Property of Ionic Hydrogel

The mechanical property of the fabricated hydrogel was investigated by tensile machine. The hydrogel showed an ultimate tensile strength of 209 kPa and a fracture strain of 1655 % with the tensile rate of 20 mm·min^{-1}, indicating that the obtained hydrogel had an outstanding elasticity (Figure S1). To investigate the diffusion behavior of ions under temperature gradient, the thermoelectric properties of the ionic hydrogel were studied firstly. Generally, the cations and anions are uniformly distributed in the hydrogel in homogeneous temperature field as the cations and anions can move freely in the ionic hydrogel. Due to the Soret effect, smaller cations tend to shift to the low temperature side when a temperature gradient is applied to the ionic hydrogel, resulting in an enrichment of cations on the low temperature side and anions on the high temperature side. As a result, the temperature difference between the two sides of the ionic hydrogel can progressively lead to a thermoelectric voltage. [41, 42]. The ionic conductive thermoelectric generator prepared in this work is essentially a capacitive thermoelectric material. Under the condition of temperature difference at corresponding ends, ions would gradually accumulate on the surfaces to

form thermoelectric voltage (Figure 2 (a)). Thermoelectric voltages of the ionic hydrogel that worked on different temperature gradients were recorded by an electrochemical workstation (Chi660e, China). In this test, the temperature of the cold side was fixed at 5 °C, and the temperature differences were set as 10, 20, 25, 30, 40 and 45 °C respectively, by tuning the temperatures at the hot end. The potential difference between the ionic hydrogel surfaces was tested under a series of temperature gradients as shown in Figure 2 (b). The potential differences between two ends of the hydrogel gradually increase and stabilize over time and they enhance with the increase of temperature variation. The linear fitting of the potential difference versus the temperature difference was shown in Figure 2 (c). The fitting curve had a regression coefficient $R^2 = 0.99889$ and a slope of 10.54 $mV \cdot K^{-1}$. The slope represents the value of ionic thermoelectric coefficient, which is very close to the previous report by our group [38], confirming the superior thermoelectric property of the hydrogel. As a result, by controlling the temperature difference at both ends of the ionic conductor, thermoelectric hydrogel can effectively achieve the selective migration behavior of anions and cations, and further obtain different kinds of ion-enriched surfaces.

The ionic conductivity was studied by electrochemical impedance spectroscopy as shown in Figure S2. The horizontal intercept of the fitted straight line represented the ionic resistance. The charge transfer resistance was converted to conductivity via the equation $\sigma = t/RA$, where σ represents the conductivity, R represents the resistance, t represents thickness of the hydrogel between two electrodes and A represents the cross-sectional area of hydrogel. In this case, the values of R, t and A were about 128 Ω, 1 mm and 0.785 cm^2, respectively. Thus, the conductivity of the hydrogel was calculated to be about 0.995 $S \cdot m^{-1}$.

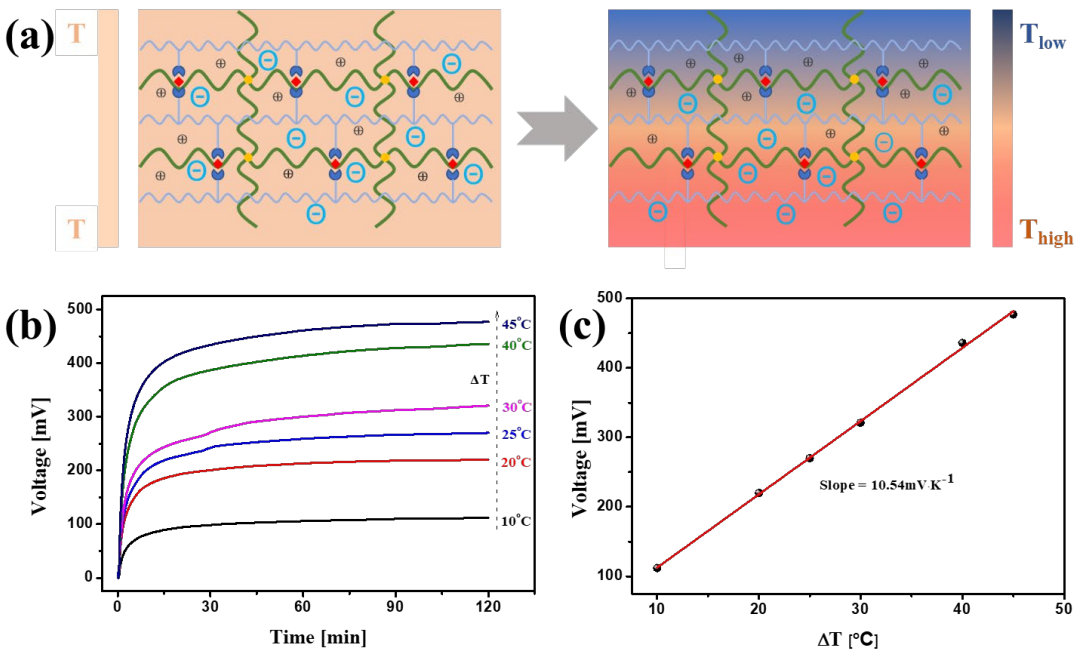

Figure 2. (a) Schematic diagram of temperature difference-induced thermal voltage in the hydrogel. (b) Thermal voltages of the hydrogel with the temperature differences of 10, 20, 25, 30, 40 and 45 °C, respectively. (c) Dependence of thermal voltages upon the temperature differences ranging from 10 to 45 °C.

2.3. Effect of Temperature Gradient on TENG Output Performance

The fabricated hydrogel-based TENG device is shown in Figure 3 (a). A commercial 3M single sided acrylic adhesive conductive fabric cloth tape coated on Cu/Ni alloy was used as the electrode, with the adhesive side firmly adhered to the ionic hydrogel. The other side of the ionic hydrogel was naturally exposed to the ambient environment and assembled into a contact-separation TENG with the conductive tape electrode. The upper polymethyl methacrylate (PMMA) board played a supporting role and controlled the contact and separation of devices through four corner springs. The electrodes affixed to the hydrogel were placed on the temperature control platform to study the effect of temperature difference on the output of the device. The temperature difference between the temperature control platform and ambient temperature was equivalent to the difference between the lower and upper surfaces of the hydrogel. In the absence of a temperature difference, the open circuit voltage of the fabricated TENG gradually expanded along with the addition of applied load, reaching 22 V under the load of 90 N (Figure 3 (b)). Under a temperature difference of 25 °C (the friction surface of hydrogel at 25 °C and the other end at 0 °C), the open circuit voltage of TENG decreases by 14 % to 19 V under a load of 90

N, compared to the scenario without a temperature difference (Figure 3 (c)). On the contrary, adjusting the heating end of hydrogel to 50 °C while maintaining the friction surface at 25 °C, the open circuit voltage of the fabricated TENG was greater than that without a temperature difference, displaying an increase of 77 % to 39 V when the load is 90 N (Figure 3 (d)). The detailed results of the output voltage are presented in Figure S3. Combined with the previous results regarding the effect of temperature difference on the material properties, we believe that the cation enriched surface of the hydrogel can induce more friction charge and higher output voltage.

The effect of temperature difference on open circuit voltage of the hydrogel-based TENG was detailed studied. The device was placed at room temperature (setting at 25 °C), and temperature of the hot stage was set at 30, 40, 60 and 70 °C, respectively. The test results are shown in Figure 3 (e-h) and the detailed data were presented in Figure S4. As the temperature difference of hydrogel surfaces increases, the output of TENG climbed up first and then declined. The increase of temperature difference leads to more cations accumulating on the hydrogel friction surface, indicating that cation enrichment favoring higher output of TENG. However, when the temperature of hydrogel surface exceeds 50 °C, the performance of hydrogel will deteriorate due to the water loss, leading to decreased output of TENG. This is consistent with other studies on hydrogel properties [43].

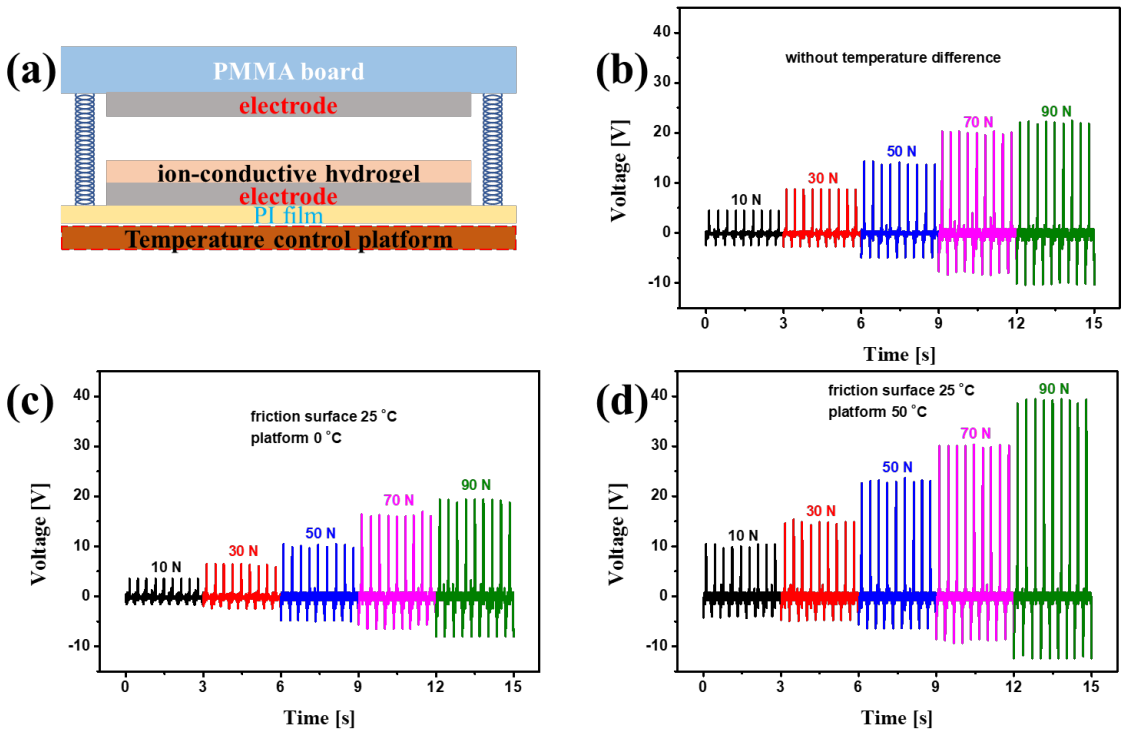

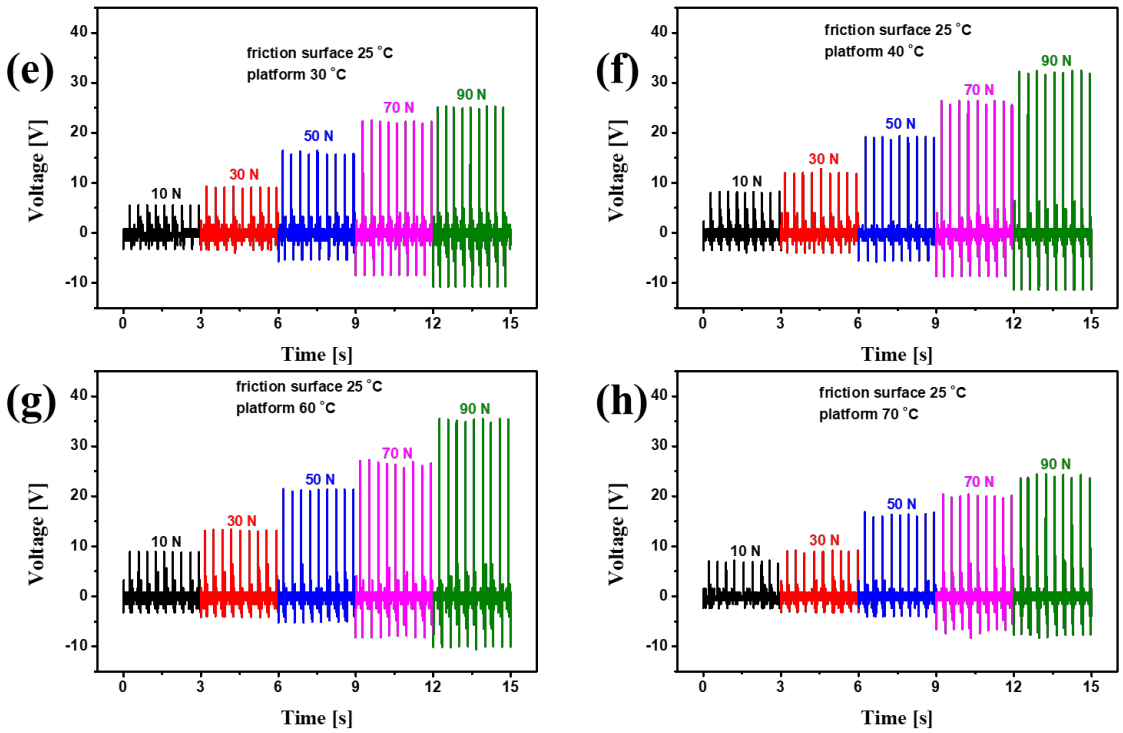

Figure 3. (a) Schematic design and fabrication of TENG via ion-enriched hydrogel. (b-h) Open circuit voltage characteristics of TENG (b) without temperature field (c) with friction surface 25 °C and the other end 0 °C of hydrogel (d) with friction surface 25 °C and the other end 50 °C of hydrogel (e) with friction surface 25 °C and the other end 30 °C of hydrogel (f) with friction surface 25 °C and the other end 40 °C of hydrogel (g) with friction surface 25 °C and the other end 60 °C of hydrogel (h) with friction surface 25 °C and the other end 70 °C of hydrogel

Further, the stability of energy conversion device is evaluated. The short-circuit current performance of the device without temperature difference and at the temperature difference of 25 °C were tested at a frequency of 3 Hz (Figure 4 (a, b)). It shows that the short-circuit current of the devices remain stable more than 5000 cycles and the short-circuit current is larger when temperature difference exists. This may be due to the flexibility and elasticity of hydrogel. Then, the friction surface temperatures of hydrogel with the temperature difference before and after testing for 30 minutes as well as the temperature of the heating platform were measured as shown in Figure S5. The results showed that after 5000 cycles testing at the frequency of 3 Hz, the temperature of the hydrogel friction surface only increased no less than 3 °C. Which can be attribute to the low thermal conductivity of the hydrogel and the good thermal conduction of the contact electrode.

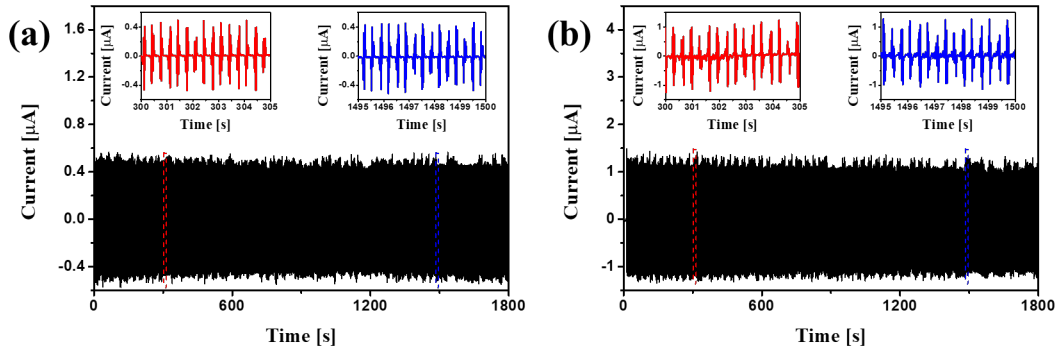

Figure 4. The short-circuit current of TENG during more than 5000 cycles at a frequency of 3 Hz (a) without temperature difference and (b) at the temperature difference of 25 °C

2.4. Effect of Cation-enriched Hydrogel Surfaces on Triboelectrification

The mechanism of ionic thermoelectric effect inducing surface ionic enriched of the hydrogel to enhance output performance of TENG is shown in Figure 5 (a). The contact triboelectrification occurred between the cation-enriched hydrogel surface and the independent top electrode when a temperature gradient existed between the upper and lower surfaces of the hydrogel. When the top electrode contacted with cation-enriched hydrogel surface, triboelectrification took place on the interface, resulting in the charge separation with the positive electrostatic charges on the top electrode and the negative electrostatic charges on the hydrogel (Figure 5 (a_1)). When the top electrode was away from cation-enriched hydrogel surface, transient electrons would flow from the bottom electrode sticking to hydrogel to top electrode, thus forming an output current (Figure 5 (a_2)). Moreover, when the top electrode reached the highest position away from the hydrogel surface, new charge equilibrium generated (Figure 5 (a_3)). Afterwards, as the top electrode moved back towards cation-enriched hydrogel surface, the operation was inverted and then an opposite direction of electron flow was created through the external resistance (Figure 5 (a_4)). The continuous alternating current signal is produced on the external circuit by repeating the above process.

The output voltage and current performances were further characterized through loading a series of resistances as shown in Figure 5 (b). It was found that the voltage at the resistance increased as the load resistance enhanced. On the contrary, the current displayed a decreasing trend with the increment of resistance. The variation trends of voltage and current with the load resistance were consistent with the results of other studies. It was worth noting that the output voltage and current were both higher at the temperature difference of 25 °C between the upper and lower surfaces of

the hydrogel. The output power density was defined by P = V × I / S (where V and I represent the voltage and current across the resistance, respectively, S is the contact area between the gel and the electrode when pressed) as given in Figure 5 (c). A highest power density about 6794 $\mu W \cdot m^{-2}$ was achieved with a resistance of 700 kΩ at the temperature difference of 25 °C. At a constant temperature, the output power density of the device was about 2553 $\mu W \cdot m^{-2}$ at 700 kΩ. The highest output power density of TENG with hydrogel on cation enriched surface increased by 166 %, laying a foundation for further application of the device.

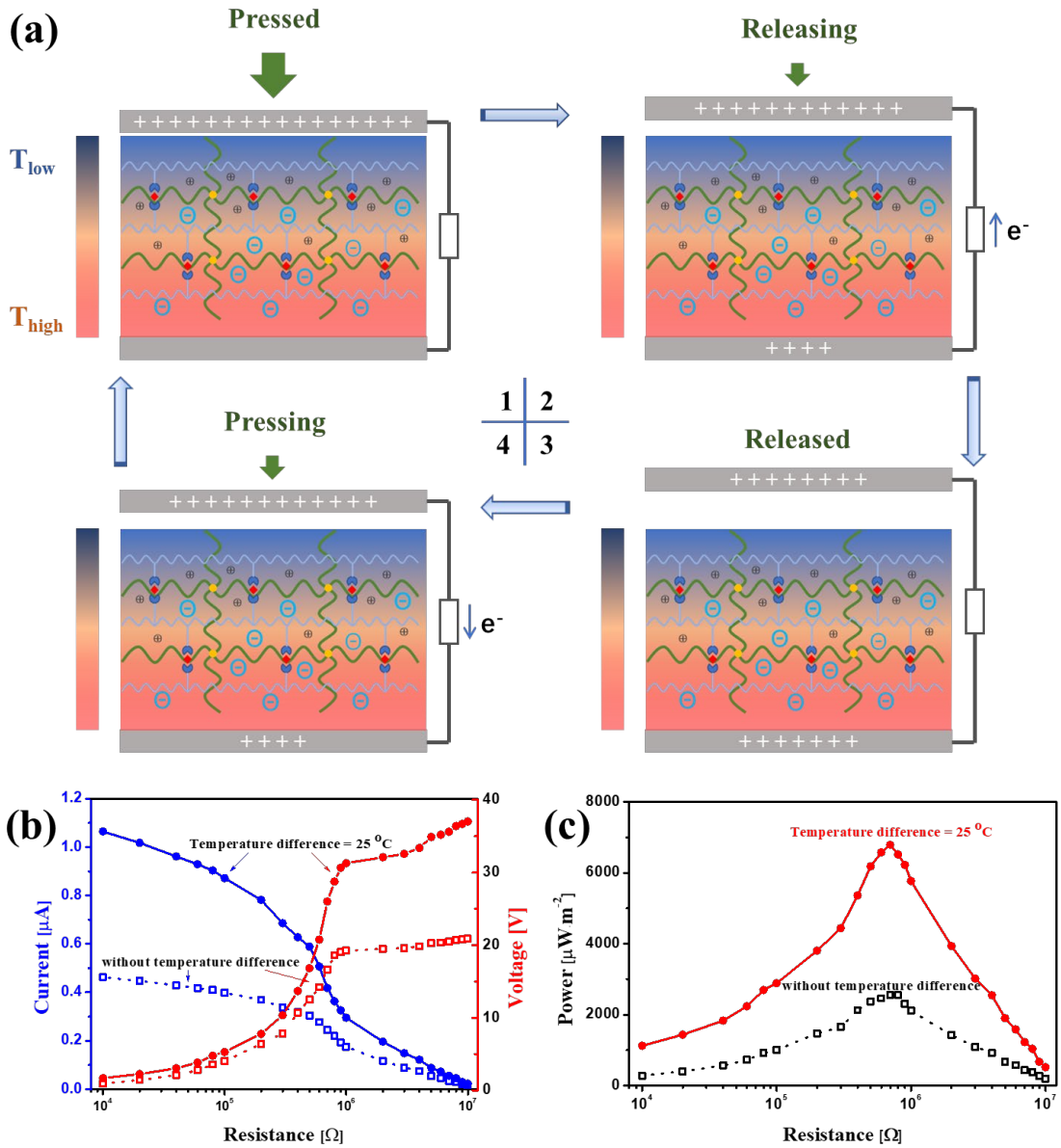

Figure 5. (a) Schematic diagram of operating mechanism of TENG, (b) Output voltage and current dependences on external load resistance with and without temperature difference, (c) Output power dependence on external load resistance with

and without temperature difference.

2.5. Application

To investigate the application of the designed TENG, a rectifier circuit was designed as exhibited in Figure 6 (a). Firstly, an intuitive and typical application of the TENG device was to intermittently power up 24 commercial LED lights installed in series when being touched by volunteer's finger (Figure 6 (b) and Supplementary Movie). The generated electricity from TENG could be stored in a capacitor for further application. The charging curves of capacitors with different capacities using the fabricated TENG (area: 4 cm × 4 cm, working frequency: 3 Hz, temperature difference: 25 °C) were shown in Figure 6 (c). It could be observed that the lower the capacitance, the faster the charging rate. Specifically, the 1.1μF capacitor could be charged to 10 V within 300 s. While the other capacitors of 1.8, 2.7, 3.9 and 4.7μF could accumulate to voltages of 8.7, 7.2, 5.3 and 4 V in turn during the same time. The harvest electricity and signal from TENG device can be used to power different kinds of wearable devices and worked as self-power sensor.

In addition, a thermal conductive polyimide (PI) film was firstly wrapped around the volunteer's arm, and the electrodes and ionic hydrogel film were laminated to the PI film. The temperature difference between the upper and lower sides of the hydrogel was created using human skin and the external environment, thereby, enrichment of ions on the hydrogel surface was achieved (Figure 6 (d)). The volunteer was asked to put on nitrile gloves and contact the ionic hydrogel surface intermittently. A single electrode TENG device can be formed in this way, and an oscilloscope was used to test the voltage across the ionic hydrogel electrodes as the nitrile gloves were scratched across the hydrogel surface. When the hydrogel material was placed on the test table with no temperature difference between the upper and lower surfaces, the open circuit voltage was 4.8 V (Figure 6 (e)). When the hydrogel material was attached to the volunteer's arm, the temperature difference between the human skin surface (about 36 °C) and the external environment (about 25 °C) resulted in an open circuit voltage of 7.2 V. Thus, the phenomenon proves that the temperature difference between human skin and environment leads to ion enrichment on the hydrogel surface, and a higher output voltage of the TENG device can be obtained.

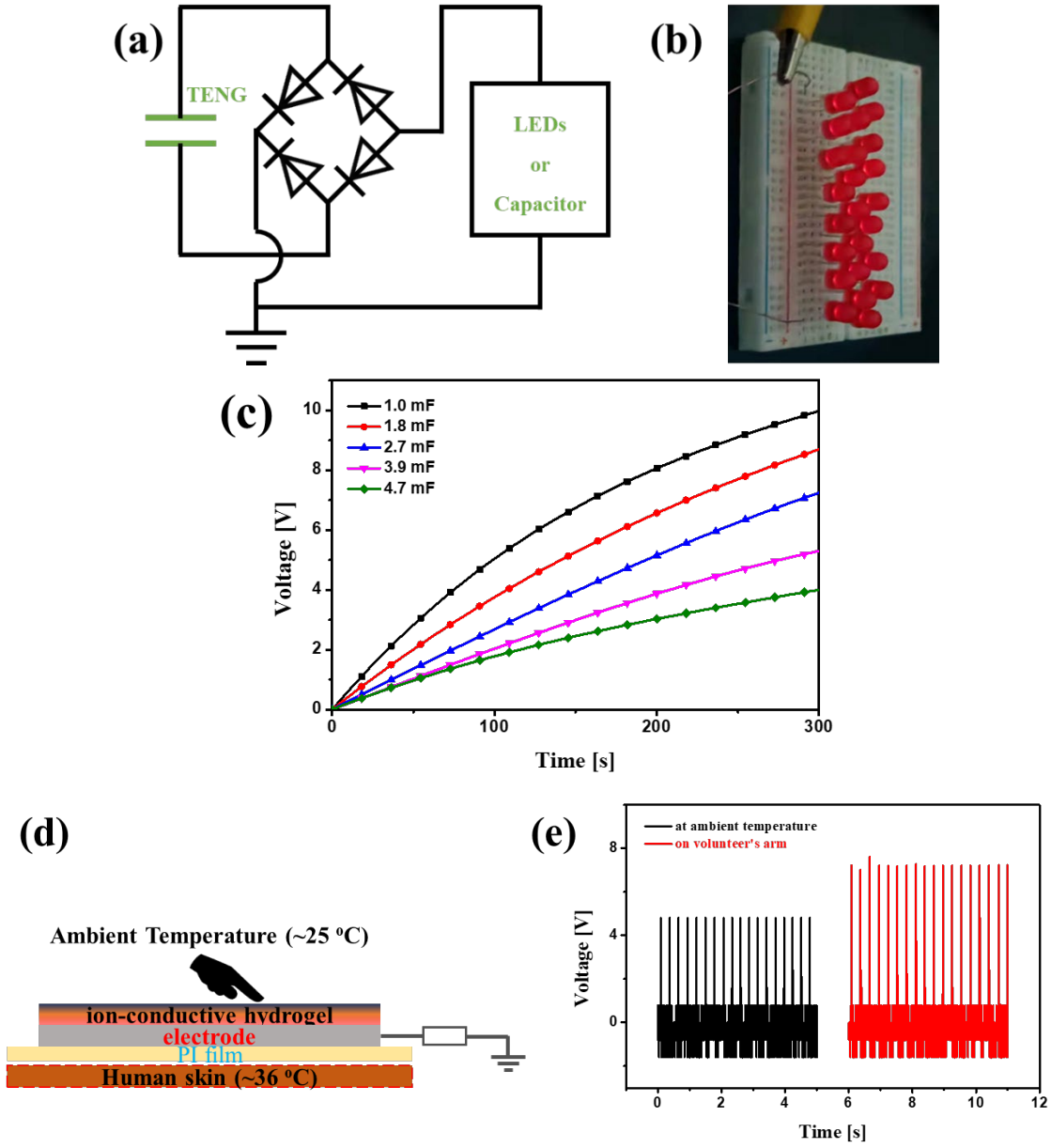

Figure 6. (a) Rectifying circuit for charging and discharging processes, (b) Digital photograph of TENG powering up 24 LED lights installed in series, (c) Charging curves for different capacitors, (d) Schematic diagram of pressing device, (e) Output voltage characteristics of device at ambient temperature.

3. Conclusion

In summary, the effect of ion-enriched hydrogel surfaces on the performance of TENG was studied for the first time. The results show that hydrogel on cation-enriched surface as the friction material favors higher open-circuit voltage. At the temperature difference of 25 °C, the open circuit voltage and maximum output power density increased by 77 % and 166 %, respectively. It has been proven that the temperature difference between human skin and the environment leads to a high open

circuit voltage, demonstrating the potential of the device for the application in wearable electronic devices. This study provides the new insights into the understanding of frictional electrification mechanism and the application of self-powered sensors.

4. Experimental Section

Materials: Acrylamide (AM, 99 %), lithium chloride (LiCl, 99 %), N, N, N', N'-Tetramethylethylenediamine (TEMED, 99 %) and *N, N′*-methylenebis-acrylamide (MBAA) were purchased from Macklin Biochemical Co., Ltd (Shanghai, China). Sodium alginate (SA), Calcium chloride ($CaCl_2$), ammonium persulfate (AP) and glycerol were purchased from Aladdin Reagent Co., LTD (Shanghai, China). Deionized water was homemade in the lab.

Preparation of hydrogel: 1 g of sodium alginate was dissolved in the miscible solvent of 49.5 g deionized water and 49.5 g glycerol in a 60 °C water bath for 4 h with stirring until a clear solution was formed. Afterwards, 10 g of the above sodium alginate solution, 8 g of AAM, 1 g of LiCl and 6 g of H_2O were mixed in a beaker at room temperature under magnetic force. The mixture was then placed in an ice water bath, followed by adding 10 mg of ammonium persulphate, 2 mg of MBAA, and 100 μL of TEMED, and cured at room temperature to form a hydrogel. Finally, the hydrogel was soaked in a 1mol·L^{-1} $CaCl_2$ solution for 1 minute, and the liquid on the surface of the gel is wiped dry for further use. For testing the thermoelectric coefficient, cylindrical hydrogel samples with the dimensions of 10 mm in diameter and 10 mm in height were used. For TENG, the dimensions of the film hydrogel sample were 4 cm long, 4 cm wide and 500 μm thick.

Fabrication of TENG: The hydrogel used for friction is attached to the commercial 3M single sided adhesive conductive fabric cloth tape, and the exposed side of the Cu/Ni alloy was used as a bottom electrode. Another tape was attached to the PMMA board as an independent top electrode. Four springs were used to separate the two electrodes, providing an air gap about 2 mm. The whole device was placed on a temperature control platform for test.

Characterization and measurement: Fourier transform infrared spectroscopy (FTIR) spectra were tested by the VERTEX70v FTIR spectrometer (Bruker, Germany). Thermoelectric effects were measured using a customized equipment

combined the temperature controller (TLTP-TEC 2415, China) with the electrochemical workstation (Chi660e, China). The ionic conductivity measurements were connected by AC impedance spectroscopy (Chi660e, China). The voltage was measured by a digital oscilloscope (Keysight InfiniiVision 4000X, America). The electrical machinery yields a controllable dynamic pushing force on the top PMMA board of the TENG at a frequency of 3 Hz.

Conflicts of interest

The authors declare no conflict of interest.

Acknowledgements

This work was supported by the National Natural Science Foundation of China (NO. 52073066), the GDAS' Project of Science and Technology Development (NO. 2021GDASYL-20210103095 and NO. 2020 GDASYL-20200102028), the Science and Technology Program of Guangdong Province (NO. 2020B0101340005), and ZQSTB's Guiding Project of Scientific and Technological Innovation (NO. 202004030110).

References

[1] W. Zeng, L. Shu, Q. Li, S. Chen, F. Wang, X. M. Tao, *Adv. Mater.* **2014**, 26(31), 5310-5336.

[2] H. Y. Zou, Y. Zhang, L. T. Guo, P. H. Wang, X. He, G. Z. Dai, H. W. Zheng, C. Y. Chen, A. C. Wang, C. Xu, Z. L. Wang, *Nat. Commun.* **2019**, 10(1), 1427.

[3] Q. Tang, H. Y. Guo, P. Yan, C. G. Hu, *Adv. Mater.* **2020**, 2(4), e12060.

[4] Y. C. Lai, H. M. Wu, H. C. Lin, C. L. Chang, H. H. Chou, Y. C. Hsiao, Y. C. Wu, *Adv. Funct. Mater.* **2019**, 29(40), 1904626.

[5] Z. L. Wang, *Adv. Energy Mater.* **2020**, 10(17), 2000137.

[6] N. Kaur, K. Pal, *Energy Technol*. **2018**, 6, 958.

[7] Z. X. Wu, X. Yang, J. Wu, *ACS Appl. Mater. Interfaces* **2021**, 13 (2), 2128-2144.

[8] X. Wang, X. H. Liu, D. W. Schubert, *Nano-Micro Lett.* **2021**,13, 64.

[9] B. W. Dong, Q. F. Shi, Y. Q. Yang, F. Wen, Z. X. Zhang, C. K. Lee, *Nano Energy* **2021**, 79, 105414.

[10] S. Y. Chen, D. Liu, L. L. Zhou, S. X. Li, Z. H. Zhao, S. N. Cui, Y. K. Gao, Y. H.

Li, Z. L. Wang, J. Wang, *Adv. Funct. Mater.* **2021**, 6(9), 2100195.

[11] H. Lei, Y. F. Chen, Z. Q. Gao, Z. Wen, X. H. Sun, *J. Mater. Chem. A* **2021**, 9, 20100-20130.

[12] Y. Lee, S. H. Cha, Y. W. Kim, D. Chol, J. Y. Sun, *Nat. Commun.* **2018**, 9, 1804.

[13] M. Pan, C. G. Yuan, X. R. Liang, J. Zou, Y. Zhang, C. Bowen, *iScience*, **2020**, 23(11), 101682.

[14] F. R. Fan, Z. Q. Tian, Z. L. Wang, *Nano Energy* **2012**, 1(2), 328-334.

[15] M. Salauddin, R. M. Toyabur, P. Maharjan, M. S. Rasel, J. W. Kim, H. Cho, J. Y. Park, *Nano Energy* **2018**, 51, 61-72.

[16] H. T. Chen, Y. Song, X. L. Cheng, H. X. Zhang, *Nano Energy* **2019**, 56, 252-268.

[17] S. W. Chen, X. Cao, N. Wang, L. Ma, H. R. Zhu, M. Willander, Y. Jie, Z. L. Wang, *Adv. Energy Mater.* **2017**, 7(1), 1601255.

[18] H. X. Wu, Z. M. Su, M. Y. Shi, L. M. Miao, Y. Song, H. T. Chen, M. D. Han, H. X. Zhang, *Adv. Funct. Mater.* **2018**, 28(6), 1704641.

[19] X. J. Cui, S. L. Cao, Z. Y. Yuan, G. Xie, J. Ding, S. B. Sang, H. L. Zhang, *Energy Technol*. **2019**, 7, 1800931.

[20] H. T. Chen, Y. Song, H. Guo, L. M. Miao, X. X. Chen, Z. M. Su, H. X. Zhang, *Nano Energy* **2018**, 51, 496-503.

[21] C. Y. Zhang, J. L. Mo, Q. Fu, Y. H. Liu, S. F. Wang, S. X. Nie, *Nano Energy* **2021**.81.105637.

[22] B. L. Cheng, Q. Xu, Y. Q. Ding, S. Bai, X. F. Jia, Y. D. C. Yu, J. Wen, Y. Qin, *Nat. Commun*. **2021**, 12, 4782.

[23] Z. H. Li, B. G. Xu, J. Han, J. X. Huang, K. Y. Chung, *Adv. Energy Mater.* **2021**, 11, 2101294.

[24] Z. D. Yu, H. Yang, N. Soin, L. M. Chen, N. Black, K. Xu, P. K. Sharma, C. Tsonos, A. Kumar, J. K. Luo, *Nano Energy* **2021**, 89, 106419.

[25] J. Park, I. Kim, J. Yun, D. Kim, *Nano Energy* **2021**, 89, 106442,

[26] H. L. Sun, Y. Zhao, C. F. Wang, K. K. Zhou, C. Yan, G. Q. Zheng, J. J. Huang, K. Dai, C. T. Liu, C. Y. Shen, *Nano Energy* **2020**, 76, 105035.

[27] A. Khan, S. Ginnaram, C. H. Wu, H. W. Lu, Y. F. Pu, J. I. Wu, D. Gupta, Y. C. Lai, H. C. Lin, *Nano Energy* **2021**, 90, 106525.

[28] H. J. Li, Y. Liang, G. R. Gao, S. X. Wei, Y. K. Jian, X. X. Le, W. Lu, Q. Q. Liu, J. W. Zhang, T. Chen, *Chem. Eng. J.* **2021**,415, 128988.

[29] Z. Chen, J. Liu, Y.J. Chen, X. Zheng, H. Z. Liu, H. Li, *ACS Appl. Mater. Interfaces* **2021**, 13(1), 1353-1366.
[30] C. H. Yang, Z. G. Suo, *Nat. Rev. Mater.* **2018**, 3(6), 125-142.
[31] J. F. Zhang, W. Xue, Y. Q. Dai, L, Wu, B. Liao, W. Zeng, X, M. Tao, *Macromol. Mater. Eng.* **2021**, 306(12), 202100486.
[32] W. Xu, L. B. Huang, M. C. Wong, L. Chen, G. X. Bai, J. H. Hao, *Adv. Energy Mater.* **2017**, 7, 1601529.
[33] X. Pu, M. M. Liu, X. Y. Chen, J. M. Sun, C. H. Du, Y. Zhang, J. Y. Zhai, W. G. Hu, Z. L. Wang, *Sci. Adv.* **2017**, 3, e1700015.
[34] D. Zhao, H. Wang, Z. U. Khan, J. C. Chen, R. Gabrielsson, M. P. Jonsson, M. Berggren and X. Crispina. *Energy Environ. Sci.* **2016**, 9, 1450-1457.
[35] H. Wang, D. Zhao, Z. U. Khan, S. Puzinas, M. P. Jonsson, M. Berggren, X. Crispin, *Adv. Electron. Mater.* **2017**, 3, 1700013.
[36] X. Shi, J. He, *Science* **2021**, 371, 343-344.
[37] C. G. Han, X. Qian, Q. Li, B. Deng, W. Liu, G. Chen, *Science* **2020**, 368, 1091-1098.
[38] J. H. Chen, L. Zhang, Y. Y Tu, Q. Zhang, F. Peng, W. Zeng, M. Q. Zhang, X. M. Tao, *Nano Energy* **2021**, 88, 106272.
[39] S. R. Pu, Y. T. Liao, K. Chen, J. Fu, S. L. Zhang, L. R. Ge, G. Conta, S. Bouzarif, T. Cheng, X. J. Hu, K. Liu, J. Chen, *Nano Lett.* **2020**, 20 (5), 3791-3797.
[40] Z. Y. Lei, W. Gao, P. Y. Wu, *Joule* **2021**, 5(8), 2211-2222.
[41] D. Desnelli, E. Eliza, A. Mara, A. Rachmat, *IOP Conf. Ser. Mater. Sci. Eng.* **2020**, 833, 012064.
[42] R. Murugan, S. Mohan, A. Bigotto, *J. Korean Phys. Soc.* **1998**, 32(4), 505-512.
[43] P. H. Yang, C. Z. Feng, Y. P. Liu, T. Cheng, X. L. Yang, H. D. Liu, K. Liu, H. J. Fan, *Adv. Energy Mater.* **2020**, 10(48), 2002898.